NFC+: Breaking NFC Networking Limits through Resonance Engineering

Renjie Zhao[1,2,*], Purui Wang[1,3,*], Yunfei Ma[1], Pengyu Zhang[1], Hongqiang Harry Liu[1], Xianshang Lin[1], Xinyu Zhang[2], Chenren Xu[3], Ming Zhang[1]

[*] Co-Primary Student Authors

[1] Alibaba Group [2] University of California San Diego [3] Peking University

ABSTRACT

Current UHF RFID systems suffer from two long-standing problems: 1) miss-reading non-line-of-sight or misoriented tags and 2) cross-reading undesired, distant tags due to multi-path reflections. This paper proposes a novel system, NFC+, to overcome the fundamental challenges. NFC+ is a magnetic field reader, which can inventory standard NFC tagged objects with a reasonably long range and arbitrary orientation. NFC+ achieves this by leveraging physical and algorithmic techniques based on magnetic resonance engineering. We build a prototype of NFC+ and conduct extensive evaluations in a logistic network. In comparison to UHF RFID, we find that NFC+ can reduce the miss-reading rate from 23% to 0.03%, and cross-reading rate from 42% to 0, for randomly oriented objects. NFC+ demonstrates high robustness for RFID unfriendly media (e.g., water bottles and metal cans). It can reliably read commercial NFC tags at a distance of up to 3 meters which, for the first time, enables NFC to be directly applied to practical logistics network applications.

CCS CONCEPTS

• **Networks** → **Network architectures**; • **Hardware** → **Wireless integrated network sensors**.

KEYWORDS

NFC, RFID, Logistics Network, Internet of Things, Magnetic Communication

ACM Reference Format:

Renjie Zhao, Purui Wang, Yunfei Ma, Pengyu Zhang, Hongqiang Harry Liu, Xianshang Lin, Xinyu Zhang, Chenren Xu and Ming Zhang. 2020. NFC+: Breaking NFC Networking Limits through Resonance Engineering. In *Annual conference of the ACM Special Interest Group on Data Communication on the applications, technologies, architectures, and protocols for computer communication (SIGCOMM '20), August 10–14, 2020, Virtual Event, USA.* ACM, New York, NY, USA, 14 pages. https://doi.org/10.1145/3387514.3406219

1 INTRODUCTION

Today's major e-commerce companies need to operate the most sophisticated logistics networks that have ever existed. Companies like Alibaba, Amazon or Walmart need to handle a package volume that is over 87 billion per year [1]. UHF RFID has been widely acclaimed to be the vital enabler that could revolutionize the digital tracking, recording, sorting and verification at the core of logistics operations. However, after numerous trials in real-world deployments, UHF RFID today only finds its use in very specific application scenarios[1]. It is unable to cover wide-ranging media and objects including food, biological, electrical, chemical, mechanical and pharmaceutical products in sophisticated logistics systems that global e-commerce companies operate.

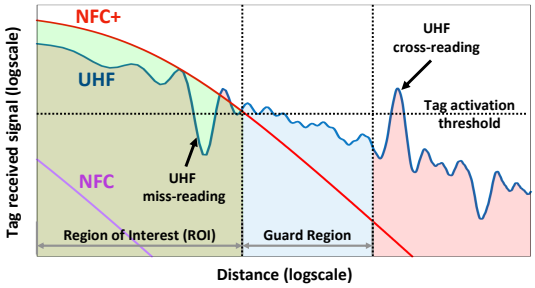

Figure 1: The propagation characteristics of the RF signal make UHF RFID unable to avoid miss-reading and cross-reading. In contrast, NFC+ leverages magnetic field to avoid miss-reading and cross-reading. Its operational range is significantly larger than NFC, which makes it suitable for logistics network applications.

Based on the operating experience of Alibaba–one of the largest e-commerce companies in the world, we demystify the reason why today's UHF RFID system does not work at large scale. The answer is simple: today's UHF RFID is just unable to achieve the 99.9% accuracy[2] needed by complex logistic networks. To have a 99.9% accuracy, an RFID system needs to achieve the following two goals at the same time.

- Read ALL (≥99.9%) the tags placed in the region of interests (ROI) as shown in Fig. 1.
- Do NOT read any (≤0.1%) undesired tags that are beyond the guard region shown in Fig. 1.

Unfortunately, current RFID systems cannot attain the two goals at the *same* time. To reliably read all the tags in ROI, an RFID system usually needs to add transmission power and improve its sensitivity, thus inevitably cross-reading undesired tags far away. To eliminate cross reading, it usually ends up missing the desired

[1]Today's major UHF RFID adopters are apparel retailers [2] such as Zara and Uniqlo whose products are most RF-friendly.

[2]On one hand, the accuracy needed by logistics network has to be extremely high. Since 87 billion packages are shipped every year [1]. With 99% accuracy, the logistics network will mis-deliver 870 million packages, which costs billions of dollars for handling mis-delivered packages. On the other hand, today's bar-code scanning achieves an accuracy of 99.9% and therefore, in order to replace bar-code at large-scale, an RFID solution with higher accuracy is desired.

SIGCOMM '20, August 10–14, 2020, Virtual Event, USA

ACM ISBN 978-1-4503-7955-7/20/08…$15.00
https://doi.org/10.1145/3387514.3406219

tags nearby. This fundamental dilemma roots in the propagation characteristics of the UHF RF signal as illustrated in Fig. 1. As many common objects including water and metal would reflect RF signals, multipath effect thereby induces unpredictable variation over path loss. We want to set a boundary about tag-reader distance (vertical line) as that of the ROI. Unfortunately, the read-or-not criterion essentially translates to a threshold of relative path loss (horizontal line). Thus the outliers along the path loss curve can cause miss- or cross-reading. Workarounds may include an extended guard zone, sometimes too large to be practical. Researchers have explored advanced near-field antennas [3], but such antennas as large as the ROI is bulky and costly. It is possible that the localization-based approach would replace the read-or-not criterion, but the localization algorithm itself is unreliable in practice under the fate of "garbage in, garbage out" [4].

In this paper, we introduce the design and implementation of NFC+, a magnetic RFID system that can address the issue of miss-reading and cross-reading. At a high level, NFC+ is made possible by rethinking how we can construct magnetic fields with multiple highly resonant coils. However, translating this high-level idea into a practical system entails multiple challenges. First, current magnetic RFID systems, such as NFC, can only operate at a short distance (typically $\leq$ 10 cm), which is not sufficient for logistic applications. Second, current magnetic RFID systems can only read a tag when it is placed with a specific orientation. NFC+ introduces the following innovations to overcome the above challenges.

First, NFC+ employs resonating magnetic coils with extremely high-quality factor (Q). We challenge the conventional wisdom that the quality factor Q should stay low (around 10) to prevent the resonance effect from distorting communication symbols [5, 6]. Instead, we choose to escalate the Q factor by orders of magnitude and re-architect the reader with separated TX and RX coils. The TX and RX coils resonate at different carrier frequencies to avoid symbol distortion. With ultra-high Q coils, much more energy can be delivered to the tag and received by the reader under the same transmit power budget, and in the meantime, the reader can also decode much weaker backscattered signals from the tag.

Second, NFC+ leverages a *passive self-interference cancellation* design to curtail the leakage from the TX chain to the RX chain that can severely impact the NFC+ reader's sensitivity and read range. In our TX/RX separating design, because the RX coil's resonant frequency deviates from that of TX coils, the high Q coil causes sharp degradation for signals that are even slightly away from the center frequency. Therefore, the leakage from TX will be significantly suppressed. Then, by combining with our novel passive narrow-band notch filter design and intermediate frequency filtering, the self-interference is minimized and the RX sensitivity is improved.

Third, we propose a novel *multi-coil magnetic beamforming* mechanism, which can fully utilize the diversity gain of multiple coils. By taking advantage of the vector field property, we prove that the NFC+ reader can "steer" its magnetic field by using multiple coils with binary phase configurations (i.e., 0 and π). This simple scanning mechanism enables the reader to cover the maximum combination.

Finally, we design *passive magnetic repeaters* to further improve the reading range and reliability. These battery-free repeaters can be excited by the magnetic field from the TX coil. Then they regenerate a complementary field to diversity the total vector field's directions and enhance its strength.

We implement NFC+ based on a custom-built hardware platform, which can directly read *standard NFC tags*. To verify its performance, we conduct microbenchmark experiments along with large-scale warehouse tests involving over 10,000 tags. The results show that:

- NFC+ can reach a maximum reading range of 3 m, whereas state-of-the-art NFC systems can only achieve 0.9 m even with the most favorable tag orientation.
- NFC+ achieves a low miss-reading rate of 0.03% when the tags are attached to various products with arbitrary orientation, in contrast to 40% and 23% in state-of-the-art NFC and UHF RFID, respectively.
- NFC+ does not cross read any tag outside of the ROI, in comparison to a cross-reading rate of 42% in UHF RFID.

To our knowledge, NFC+ represents the first system to solve the cross-reading and miss-reading problem that has plagued RFID for decades in realistic deployment. We believe that NFC+ paves the way towards deploying RFID at scale in logistics networks.

2 MOTIVATION AND BACKGROUND

2.1 Rethink RFID system design

The miss-reading and cross-reading problems are direct consequences of the intrinsic physical nature of UHF radio waves. In order to overcome this challenge, we argue that we should rethink the design of today's logistic RFID systems at a fundamental level. Specifically, instead of relying on electromagnetic radio waves, we propose NFC+ to harnesses magnetic signals and re-architect RFIDs in logistic networks. NFC+ embraces the magnetic nature of near field communication (NFC) and transforms these short-range battery-free NFC tags into long-range and reliable RFIDs. NFC+ exploits NFC for the following immediate advantages:

- NFC relies on 13.56MHz magnetic signal for communication, which can easily penetrate all kinds of media that would block or reflect RF signals including liquid and even metallic objects[3].
- Magnetic signal is non-radiative, and its "energy" degrades at $O(1/d^6)$ with distance d, much faster than $O(1/d^2)$ for RF signal. In addition, a magnetic signal rarely experiences multipath reflection, which prevents cross-reading undesired tags beyond the operating range.
- NFC tags are battery-free and extremely low-cost. Similar to UHF RFID, NFC relies on energy harvesting and does not require a battery for operation. In addition, NFC tags have already been produced on a massive scale. The cost of an NFC tag has been made as low as 5 cents [7], comparable to UHF RFID tags[4].
- NFC is well supported by multiplexed protocols such as ISO 15693 and ISO 14443, which allow multiple tags to be read simultaneously. The read rate is more than 50 tags/s which is sufficient for logistic applications.

[3] Thin and non-ferromagnetic, *e.g.,* aluminum foil.

[4] Note that due to application difference, today's NFC chips have more memory volume than UHF RFID. We expect the cost of the NFC tag to further shrink down if NFC tags are applied to logistics.

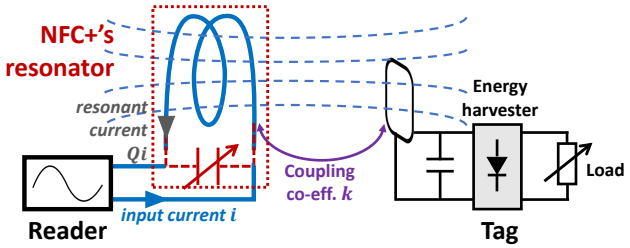

Figure 2: NFC reader-tag setup and close-loop magnetic coupling when tag is close to the reader. NFC+ leverages an additional high-Q resonator (simplified as the paralleled shunt inductor and capacitor) which builds on top of NFC to boost range.

2.2 Physics behind NFC and its limitations

Unfortunately, today's NFC systems are fundamentally crippled by its communication range. Current NFC systems are designed following the principles of inductive magnetic coupling [8]. As shown in Fig. 2, an NFC reader usually employs a loop antenna to elicit magnetic fields while NFC tags also employ small coils to pick up the produced magnetic fields. When the reader's fields traverse a tag's coil. The NFC reader and the tag are inductively coupled with each other via a magnetic field, so the antennas between the reader and the tag effectively form a transformer with a specific coupling coefficient k which is a function of the tag's location and orientation. The reader delivers power and commands to the tag through the transformer and detects the load changing when the tag is doing load modulation. However, in such an inductively coupled system, when a tag is placed slightly away from the reader or has a small degree of undesired orientation, the coupling coefficient k quickly diminishes, leading to loose coupling between the reader and the tag, which impedes the tag's energy harvesting and data communication. Therefore, NFC systems that are built based on inductive coupling typically only operate with a range of less than 10 centimeters [9].

2.3 Resonance effect and quality factor

To fundamentally overcome the limited communication range in the current NFC system, NFC+ builds on top of a physical phenomenon called *Resonance*, which is the amplification that occurs when a signal is applied at the natural frequency of a system. In order to leverage the resonance effect, a resonator is required as shown in the red block of Fig. 2. Because the size of the loop antenna is relatively small compared to the NFC carrier wavelength (22 m), the input current is evenly distributed on the loop [10]. Hence, the loop antenna itself can be regarded as a discrete inductor and resistor. To form a resonator, an additional capacitor is added across the loop antenna. The energy in a resonator is stored in two different ways: (1) the electrical energy as charges accumulate at the capacitor electrodes and (2) magnetic energy as currents flow through the inductor. There is a tendency of such two types of energy converting into one another, causing oscillation between the capacitor and the inductor. The natural frequency of such oscillation is decided by:

$$f_0 = \frac{1}{2\pi\sqrt{LC}} \tag{1}$$

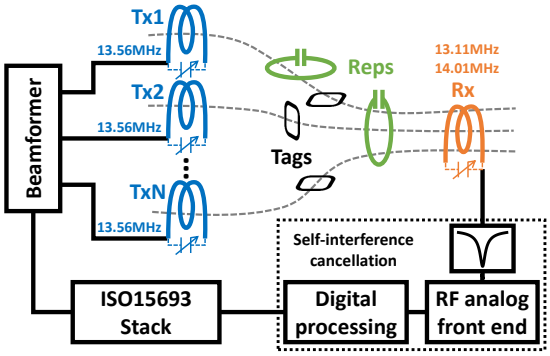

Figure 3: NFC+'s system overview

By changing the value of the capacitor, we can tune the resonant frequency to 13.56 MHz in NFC. The strength of such oscillation is measured by an important physical parameter called quality factor (Q) [11], which is defined as the ratio of the peak energy stored in the resonator to the energy lost per radian in a cycle of oscillation. In an RLC parallel circuitry, Q can be calculated as:

$$Q = \frac{R}{2\pi f_0 L} \tag{2}$$

When an input current is fed into a resonator, the resonant current passing through its coil will be Q× of the input current, which means that magnetic field strength is amplified by Q× compared to a resistive load even though the input power stays the same. However, it is worth noting that there is also a trade-off between the frequency, bandwidth, and Q, which can be written as:

$$BW = \frac{f_0}{Q} \tag{3}$$

The above equation tells that the communication bandwidth is inversely proportional to the quality factor of the resonator. As a result, in communication, a high Q system is rarely employed due to the bandwidth constraint it imposes on sending and receiving data.

3 NFC+ SYSTEM OVERVIEW

Fig. 3 summarizes the key components in NFC+. To extend the range where a tag can operate, we physically separate transmission and reception coils and leverage high quality factor coils for both transmission and reception. However, TX coils are tuned to resonate around 13.56 MHz while the RX coil will resonate around 13.11 MHz or 14.01 MHz. In addition, we design passive self-interference cancellation circuit to enable the reader to receive and decode very weak backscattered signal when a tag is far away from the reader. Then, we leverage multiple TX coils to realize efficient magnetic beamforming to ensure tags with undesired orientations can also obtain sufficient power for its operation. Finally, we design passive (batteryless) repeater which is deployed at locations close to the tag and helps read tags far away from the TX coil or with undesired orientations. We will introduce the design of each component in the following sections.

4 PUSHING RANGE LIMITS

In this section, we will describe how NFC+ leverages high-quality factor coil, TX/RX separated transceiver design and self-interference

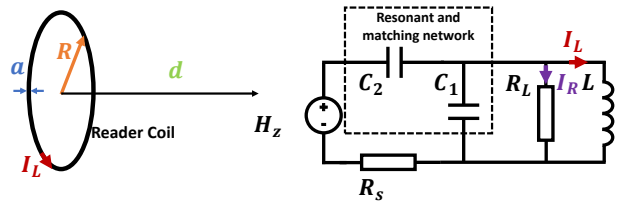

(a) Current loop model of a reader coil. **(b)** The equivalent circuit model.

Figure 4: The physical model and the equivalent circuit model of a reader coil.

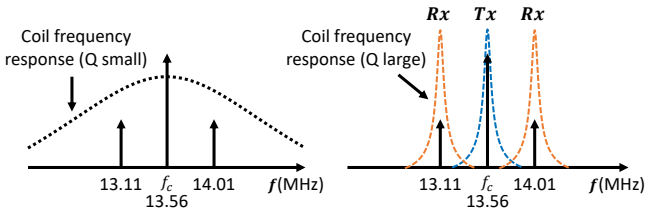

(a) Coil frequency response when Q is small **(b)** Coil frequency response when Q is large

Figure 5: Frequency response of coils with different quality factors. To use high Q coils, we use different coils for transmission and reception. The TX coils are tuned to 13.56 MHz and the RX coils are tuned to 13.11 MHz or 14.01 MHz.

cancellation techniques to significantly boost the operational range of NFC systems.

4.1 Why we need high quality factor coils?

We start by modeling the magnetic field generated from a reader coil. The goal is to identify the fundamental design knobs that determine the field strength. Without loss of generality, we model the coil as a circular loop carrying current I_L, as shown in Fig. 4a. The equations corresponding to different coil shapes are slightly different, but our conclusion still holds regardless. Since the coil size is much smaller than the signal wavelength, the current I_L can be considered as evenly distributed, and hence we can use a static magnetic model to analyze the system [12]. Following the Biot-Savart law [13], the field along the coil's central axis is:

$$H_z = \frac{R^2 I_L}{2(d^2+R^2)^{\frac{3}{2}}} \tag{4}$$

where d is the distance between reader coil and tag and R is the radius of the coil.

Because the reader coil is a "small loop" comparing to the 22 m wavelength, the reader coil can be treated as an inductor L shunted with a resister R_L. Then, taking a simple resonant and matching network which is used to form a resonator and match the coil impedance to the voltage source internal resistance R_s, the reader can be simplified as the circuit in Fig. 4b, the current I_L is related to the reader's output power P and the quality factor Q of the coil. The reader coil's inductance can be calculated as [14]:

$$L \propto R\left[\ln\left(\frac{8R}{a}\right)-2\right] \tag{5}$$

where a is the wire radius. The resistance R_L is made tunable to achieve different Q values with the same L. Given a specific Q, $R_L = \omega_c LQ$. If the matching is perfect, R_L is loaded with half of the available power from the signal source, which is P and the current through R_L is $I_R = \sqrt{\frac{P}{R_L}} = \sqrt{\frac{P}{\omega_c LQ}}$. Therefore, we have:

$$I_L = QI_R = \sqrt{\frac{PQ}{\omega_c L}} \tag{6}$$

Then, the magnetic field generated by a reader passing through the tag can be modeled as:

$$H \propto \sqrt{\frac{PQ}{R\left[\ln\left(\frac{8R}{a}\right)-2\right]}}\frac{R^2}{(d^2+R^2)^{\frac{3}{2}}} \tag{7}$$

The field strength H depends on the following factors: reader transmission power P, reader coil radius R, coil quality factor Q, coil wire radius a and distance d. *Obviously, to achieve longer distance d, we may increase P, R, a or Q.*

However, simply increasing the transmission power P will cause severe safety problems. The most powerful state-of-the-art commercial NFC reader [15] has 8 Watts output power and offers a maximum read distance up to 0.9 m. To extend the reading distance to 3 m, the reader's output power needs to reach an alarming level of $8\times(\frac{3}{0.9})^6 = 11$ kW, which is hardly achievable by practical power source and dangerous for human operators [16]. The reason roots in the fact that P is proportional to d^6 as shown in Eq. 7. Similar to P, increasing the wire radius a is not a viable solution, either. To reach 3 m distance, wire radius needs to be increased by $e^{(\frac{3}{0.9})^6} = e^{1372}$ times, which is infeasible in practice.

Another idea is to play with the geometry R. An optimal R can be calculated by setting the derivative of Eq. 7 to zero, which leads to an R comparable to d. Unfortunately, abusing R is also infeasible for two reasons: (1) A large coil has a high self-inductance, which can only function under small resonating capacitance when the coil is tuned to 13.56 MHz as shown in Eq. 1. The small capacitance can be easily affected by parasitic capacitance which is induced from nearby environment. As a result, the coil would get detuned from the desired 13.56 MHz frequency even though it has been carefully calibrated in the lab settings. (2) To efficiently elicit magnetic fields from the source, the loop currents shall be evenly distributed along the coil to avoid spurious electromagnetic emission at far-field [17], which implies that the maximum circumference of the coil can only be a small fraction of the wavelength λ ($< 0.1\lambda$ as a rule of thumb [17]). As a result, in practice, R has to be limited to around 0.5 m.

The above analysis implies that the quality factor Q of a coil remains as the major factor that can be practically leveraged to extend the range. A Q value on the order of several hundred is feasible since the internal resistor of a coil can be made very small. This kind of high Q loop antenna has been well studied in amateur radio [18]. Unfortunately, a commercial NFC reader coil typically employs a very small Q factor of around 8 by adding an additional resistor [5]. Such a design was made to ensure that the same coil can be used simultaneously for wireless power transfer and bidirectional data communication.

Fig. 5 shows how the quality factor of a coil impacts data communication. In the ISO 15693 NFC protocol, a tag talks to a reader through sideband modulation with a sub-carrier of 423.75 kHz or 484.25 kHz. To decode the tag's signal with 13.56 MHz carrier received by the same transmitting coil, the sampling bandwidth

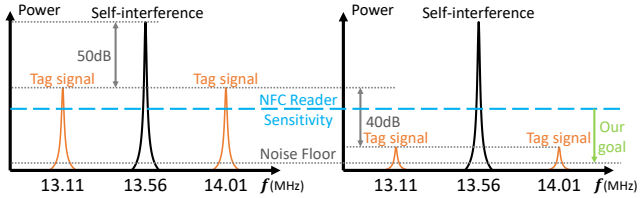

(a) Received signal strength when tag is 10cm away

(b) Received signal strength when tag is 1m away

Figure 6: Self-interference experienced by a reader when a tag is placed at different distances from the reader.

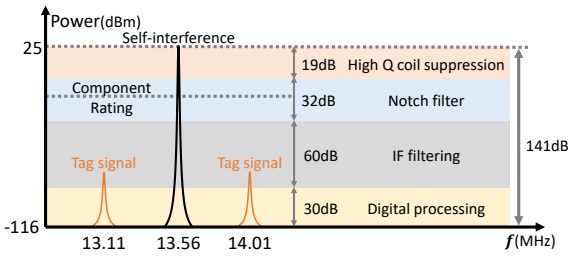

Figure 7: NFC+ uses high Q coils, notch filters, IF filters and digital baseband processing for self-interference cancellation.

needed is around 484.25 kHz × 2 ≈ 1 MHz. Since bandwidth BW of a coil is inversely proportional to its quality factor $Q = f_c/BW$, the Q of the coil should be no more than 13.56 MHz/1 MHz = 13.56. A typical practice is to employ a $Q = 8$ so that it can also support ISO-14443 which has larger sub-carrier frequency. Using such a small Q, the frequency response of the coil is not sharp and its bandwidth is wide as shown in Fig. 5a. Therefore, tag-to-reader data communication can sustain.

Although Eq. 7 tells us that a large Q improves the magnetic strength, the frequency response of the coil becomes sharp as shown by the blue dotted curve in Fig. 5b. As a result, the tag-to-reader communication suffers because the frequency of the backscattered signal sits outside of the bandwidth of the coil. How to increase the Q factor without compromising the communication link?

4.2 Support high Q coils via T/R separation

Instead of using a single coil for both transmission and reception, NFC+ achieves high-quality factors by using at least two coils, one for transmission and one for reception. We do so because we want to unleash the power of Q by decoupling transmission and reception.

Let us first look at the quality factor of the TX coil. The reader-to-tag downlink transmission adopts pulse position modulation with an $T_b = 9.44\ \mu s$ pulse width (ISO-15693 protocol), which suggests that the bandwidth required for reader-to-tag link is around $1/T_b = 106$ kHz. [10] Since the center frequency of the TX coil is around 13.56 MHz, the Q of the TX coil can be increased to 13.56 MHz/106 kHz = 128, 16× larger than that of a typical commercial NFC reader.

Unlike commercial NFC systems where RX operates around 13.56 MHz, as shown in Fig. 5b, we tune the RX coil to operate around 13.11 MHz or 14.01 MHz, corresponding to the lower/upper sideband frequencies used in the tag-to-reader communication link. The tag performs FSK modulation at 6.7 kbps with a 423 kHz or 484 kHz subcarrier. The minimum sampling bandwidth required by the reader to decode the information is $(484 - 423) + 2 \times 6.7 = 74.4kHz$. As a result, the RX coil can have a $Q = 14.01$ MHz/74.4 kHz = 188. Overall, using a $Q = 128$ TX coil and a $Q = 188$ RX coil can extend the reader-to-tag link range by 1.6× and tag-to-reader link range by 1.7× compared to the $Q = 8$ coils used by state-of-the-art commercial NFC readers.

4.3 Passive self-interference cancellation

To further increase the link budget and boost the range, we need to handle self-interference to improve the RX sensitivity. This RX side improvement is needed because the strength of reader received signal will suffer two times of "path loss" and easily become bottleneck when distance increase. Self-interference, which is the leakage from the TX to the RX chain, is one of the main factor that limits the RX sensitivity. In this section, we will discuss why this issue is not solved in commercial NFC systems and how we can use simple passive circuits to address the problem.

Commercial NFC readers do not have self-interference cancellation circuits mainly because it is unnecessary to have a sensitive receiver for short-range (≤10 cm) applications [9]. To understand the impact of self-interference, we use the Tagformance Pro platform from Voyantic [19] to measure the tag signal strength as well as the strength of self-interference by feeding the RX path into a spectrum analyzer. The results are illustrated in Fig. 6. When a tag is 10 cm away from the reader, the backscattered signal is only about 50 dB lower than the self-interference from the reader and is well above the noise floor. Therefore, the majority of commercial readers with amplitude and phase detectors [20] performing non-coherent demodulation [21] can still successfully decode the tag signal even without self-interference cancellation.

However, when the tag moves away from the reader, the backscattered signal becomes very weak while self-interference remains the same. Following the model in Eq. 7, when the tag-to-reader distance moves from 10 cm to 1 m, the strength of the tag's backscattered signal will decrease by 40 dB [5]. As illustrated in Fig. 6, the backscattered signal will be much lower than the self-interference. In such a condition, self-interference cancellation becomes important to design a near-to-noise-floor sensitivity receiver.

NFC+ introduces a simple but novel passive circuit to address this issue. Our passive circuit includes *three parts*: high Q coil suppression, notch filter and IF filter. We first explain how we use high Q coils to suppress the self-interference. As discussed in Sec. 4.2, we tune the TX coil and RX coil to operate around 13.56 MHz and 14.01 MHz (or 13.11 MHz), respectively. Because of the bandwidth and Q trade-off in Eq. 3, the high Q RX coil will suppress the signal outside 14.01 MHz (or 13.11 MHz) band. As a result, the 13.56 MHz self-interference from the TX coil will be suppressed by the high-Q RX coil. To illustrate such a high-Q suppression effect, we used two high Q coils separated by 2 m and measure the self interference when the RX coil is tuned to 13.56 MHz and 14.01 MHz, respectively. The results are shown in Fig. 7. We can see that the combination of high Q TX and RX coils can suppress the strong self interference by 19 dB. Note that such a 19 dB suppression is extremely important

[5] The maximum read range of Tagformance Pro is 30 cm. Therefore, we calculate signal strength at 1m based on measured results at 10 cm.

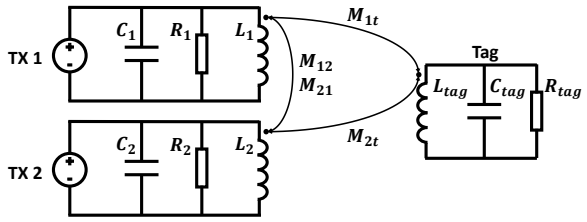

Figure 8: Circuit model of two TX coils setup.

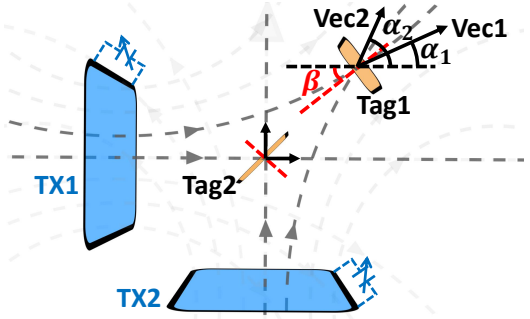

Figure 9: Two perpendicular TX coils setup and the vectors on the coordinate system.

since it deals with high-power jamming signals which may damage the following components.

Even though the self-interference is reduced by 19 dB, the remaining self-interference is still very large compared to a tag's backscattered signal and also higher than the component rating power which may destroy the front-end components in a receiver. One may consider using the active cancellation techniquein UHF RFID and full-duplex communication systems to further suppress the self-interference [22]. Active cancellation can be achieved by controlling the phase and amplitude of a copy of signal from the TX chain, so as to produce a signal which is exactly the opposite of the interference signal. However, during the procedure of searching such an opposite phase and amplitude, the coupled signal might get constructively combined with the self-interference and cause damage to the component.

To overcome the barrier, our key insight is that the frequency of the excitation signal is relatively low (13.56 MHz). Therefore, we design a crystal notch filter that has 15 dB sharp rejection around 13.56 MHz and very low loss (less than 1 dB) near 13.10 MHz or 14.01 MHz. In addition, we cascade several notch filters to achieve near 32 dB interference rejection. Combining high Q coils and cascaded notch filters, the self-interference is suppressed by 50 dB.

In addition to passive circuits described, NFC+ leverages IF filtering and digital baseband processing, such as digital filtering, to further suppress the self-interference. The overall 141dB self-interference suppression can reduce the self-interference near to the -120 dBm thermal noise floor, which makes the reader sensitive enough for decoding a weak backscattered signal even when the tag is far from the reader.

5 INVENTORY MISORIENTED TAGS

Another limitation of existing NFC systems is that a reader can only read tags with specific orientations. In this section, we introduce how NFC+ leverages multi-coil diversity to meet the challenge. We note that existing NFC systems are designed to work in short range only and a single coil suffices. A multi-coil system entails non-trivial design choices to maximize diversity gain and avoid destructive interference.

5.1 Model of multi-coil system

NFC+ borrows the high-level idea of antenna diversity from far-field radar systems, which sweep through beam patterns to broaden the angular coverage. But in doing so, we must first deal with the mutual inductance intrinsic to near-field communication systems. As shown in Fig. 8, the mutual inductance exists between (1) the reader and the tag, e.g. M_{1t}, M_{2t} and (2) the reader's multiple coils, e.g. M_{12}, M_{21}. From a circuit perspective, mutual inductance creates additional load to a signal source which in turn affects the current amplitude and phase distributed on the reader coil. In Appendix A, we show the mutual inductance between the reader coils can be accounted for without compromising the simplicity of our model, so that we could treat the TX coils as uncoupled "current loops". On the other hand, the tag-to-reader mutual inductance is much smaller compared to that of the reader coils. Therefore, the loading effect caused by the tag to the reader can be ignored.

Another issue is that unlike the electromagnetic wave in the far-field, the magnetic field is a vector instead of scalar. Therefore, in what follows, we explicitly model and discuss the behaviour of magnetic field signal. As illustrated in Fig. 9, The currents on TX1 and TX2 produce magnetic field $\vec{H}_1$ and $\vec{H}_2$ at Tag1's location $\mathcal{R}$, respectively. α_1 and α_2 denote the corresponding vector directions of $\vec{H}_1$ and $\vec{H}_2$. Then the two vectors at n^{th} time slot can be expressed as:

$$\begin{aligned}\vec{H}_1(n,\mathcal{R}) =&[a_1(n,\mathcal{R})sin(\omega t+\phi_1(n))cos(\alpha_1(\mathcal{R})),\\ &a_1(n,\mathcal{R})sin(\omega t+\phi_1(n))sin(\alpha_1(\mathcal{R}))]\\ \vec{H}_2(n,\mathcal{R}) =&[a_2(n,\mathcal{R})sin(\omega t+\phi_2(n))cos(\alpha_2(\mathcal{R})),\\ &a_2(n,\mathcal{R})sin(\omega t+\phi_2(n))sin(\alpha_2(\mathcal{R}))]\end{aligned} \tag{8}$$

where $a_i(n,\mathcal{R})$ and $\phi_i(n)$ denote the magnitude and phase, respectively. The magnitude depends on the location $\mathcal{R}$ and the excitation current whose magnitude is $A_i(n)$. The amplitude can be further expressed as the multiplication of a location-dependent factor and a time-varying factor, i.e., $a_i(n,\mathcal{R}) = k_i(\mathcal{R})A_i(n)$. The phase is determined by the excitation current phase $\theta_i(n)$ on the TX coils. In the near field regions, *the phase change introduced by propagation can be ignored [12] which implies* $\phi_i(n) = \theta_i(n)$. Then the combined magnetic field $\vec{H}_s(n)$ can be written as:

$$\begin{aligned}\vec{H}_s(n,\mathcal{R}) =&[k_1(\mathcal{R})A_1(n)sin(\omega t+\theta_1(n))cos(\alpha_1(\mathcal{R}))\\ &+k_2(\mathcal{R})A_2(n)sin(\omega t+\theta_2(n))cos(\alpha_2(\mathcal{R})),\\ &k_1(\mathcal{R})A_1(n)sin(\omega t+\theta_1(n))sin(\alpha_1(\mathcal{R}))\\ &+k_2(\mathcal{R})A_2(n)sin(\omega t+\theta_2(n))sin(\alpha_2(\mathcal{R}))]\end{aligned} \tag{9}$$

Let β denote the angle of the normal of the tag plane. We show in the Appendix B that from Eq. 9 and by using $\theta_1(n)$ as the phase reference, the power of the combined signal received by the tag can be written as:

$$\begin{aligned}P_{B,2}(n,\mathcal{R},\beta) =&\big(b_1(n,\mathcal{R},\beta)+b_2(n,\mathcal{R},\beta)cos(\theta_2(n)-\theta_1(n))\big)^2+\\ &\big(b_2(n,\mathcal{R},\beta)sin(\theta_2(n)-\theta_1(n))\big)^2\end{aligned} \tag{10}$$

where $b_i(n,\mathcal{R},\beta) = S_i k_i(\mathcal{R})A_i(n)cos(\alpha_i(\mathcal{R})-\beta)$, S_i is a factor corresponding to the property of the tag, such as coil size, number of

turns etc. When extending to N TX coils, the tag received signal power will be:

$$P_{B,N}(n,\mathcal{R},\beta) = \big(b_1(n,\mathcal{R},\beta) + \sum_{i=2}^{N} b_i(n,\mathcal{R},\beta)cos(\theta_i(n)-\theta_1(n))\big)^2 + \big(\sum_{i=2}^{N} b_i(n,\mathcal{R},\beta)sin(\theta_i(n)-\theta_1(n))\big)^2 \tag{11}$$

From the equation above, it can be seen that the final signal strength associated with a specific location and orientation is determined by the amplitudes $A_i(n)$ and the phases $\theta_i(n)$ of TX coils. As a result, we could borrow the codebook concept from far-field RF beamforming [23]. In particular, we design a two-dimension codebook the n^{th} entry of which represents a $(A_i(n), \theta_i(n))$ combination. Then, by iterating over the different entries, we are able to cover the whole spatial region. In the following section, we introduces the detailed codebook design.

5.2 Magnetic beamforming

In its simplest form, the codebook is designed as follows: the amplitude $A_i(n)$ should take the maximum available value and remain the same across the codebook; the phase should take all the permutation of $\theta_i - \theta_1 = 0$ or π, $k = 2 : N$.

The amplitude design choice is straightforward since larger $A_i(n)$ means larger $b_i(n,\mathcal{R},\beta)$. Therefore, we will mainly focus on proving how the phase design can cover all the maximum combination. It is noteworthy that the following proof applies to arbitrary tag location and arbitrary orientation, because they only influence the amplitude value $b_i(n,\mathcal{R},\beta)$. We will thus remove $\mathcal{R}$ and β to ease the exposition.

Starting with 2 TX coils, by taking the derivative of Eq. 10 with respect to the phase difference $\Delta\theta_2(n) = \theta_2(n) - \theta_1(n)$, we can see that $P_{B,2}(n)$ is maximized when $\Delta\theta_2(n)$ equals 0 or π. Therefore, the two TX coils only need to try two values of $\Delta\theta_2(n)$, *i.e.,* 0 or π, in order to identify the phase offset configuration that achieves optimal magnetic beamforming.

Now, we prove when extending the number of TX coils to N based on Eq. 11. By controlling the phase difference between the ith coil and the 1st coil $\Delta\theta_i(n) = \theta_i(n) - \theta_1(n)$ and traversing $\Delta\theta_i(n) = 0$ or π, N TX coils can deliver the following amount of power to a tag:

$$P_{B,N,0+\pi}(n) = \big(|b_1(n)| + \sum_{i=2}^{N} |b_i(n)|\big)^2 \tag{12}$$

Next, we prove $P_{B,N,0+\pi}(n)$ is maximum. By subtracting $P_{B,N}(n)$ from $P_{B,N,0+\pi}(n)$, we get

$$\begin{aligned} &P_{BN,0+\pi}(n) - P_{BN}(n) \\ &= 2|b_1| \sum_{i=2}^{N} |b_i(n)|\big(1 - sign(b_1(n)b_i(n))cos(\Delta\theta_i(n))\big) \\ &+ 2\sum_{i\neq j} |b_i(n)||b_j(n)|\big(1 - sign(b_i(n)b_j(n))cos(\Delta\theta_i(n) - \Delta\theta_j(n))\big) \end{aligned} \tag{13}$$

where $sign(\cdot)$ indicates the sign of a number. Since both sign value $sign(b_1(n)b_i(n))cos(\Delta\theta_i(n))$ and $sign(b_i(n)b_j(n))cos(\Delta\theta_i(n) - \Delta\theta_j(n))$ are smaller than 1, we have $P_{B,N,0+\pi}(n) \geq P_{B,N}(n)$. Therefore, N TX coils can deliver the maximum amount of power to tags by setting the phase of each TX coil to either 0's or π's. In practice, an $N \leq 6$ will suffice for activating the tags in the region of interests. Hence, the codebook size (or searching complexity) for NFC+'s beamforming system is just $2^{N-1} \leq 32$, which can be sweeped through in a very short amount of time.

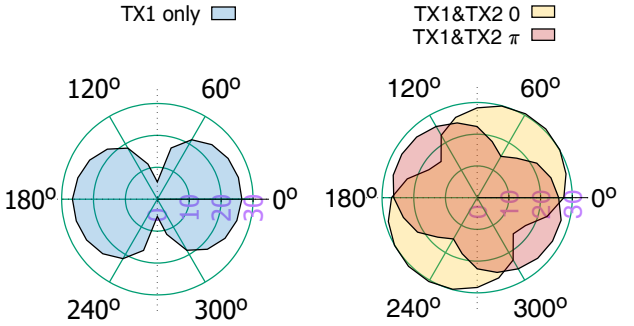

(a) Single TX coil **(b) Two TX coils with 0 or π phase difference.**

Figure 10: Beam patterns when using a single TX coil and two coils with magnetic beamforming.

We now conduct a simple experiment to illustrate the effectiveness of NFC+'s magnetic beamforming. Using the setup in Fig. 9, we place a pick up loop at the tag2 location. Then, we rotate the pickup loop while measuring the captured signal strength. We compare our beamforming method with the single coil setup. Fig. 10 shows that a single fixed $\Delta\theta$ cannot cover all of the orientations which explains why commercial NFC cannot read tags with undesired orientations. In our case, by switching between $\Delta\theta = 0$ and $\Delta\theta = \pi$, our magnetic beamforming algorithm is able to achieve the strongest strength across all the orientations.

6 PASSIVE MAG-REPEATER

The real-world environments of logistics operations are dynamic and unpredictable. To overcome the "last mile" challenge and achieve overall reliability > 99.9%, NFC+ further introduces a magnetic repeater (mag-repeater) to compensate range and angle coverage and eliminate "dead spots". With the help of the mag-repeater, NFC+ is able to deliver energy and communicate to tags that are trapped in extremely unfavorable conditions. Unlike the conventional RF relays [24], *the NFC+'s mag-repeater is a passive, battery-free device.* Specifically, as illustrated in Fig. 11, mag-repeater is a one-turn coil (in green color) that is remotely coupled to either the TX or the RX coils of the reader (in blue color). The mag-repeater forms a "slave-master" relationship with the reader and spontaneously repeats a reader's action even though it does not have a battery. The passive nature of NFC+'s mag-repeater allows it to be easily deployed in various harsh environments. In the following analysis, we will show how this mag-repeater interacts with the TX coil and how it can act like an independent TX coil without the need of active components. The analysis focuses on the TX but it also applies to the RX.

As shown in Fig. 12a, suppose a reader's TX coil produces a magnetic field flux that passes through the one-turn circular repeater coil denoted in green color with radius R_{rep}. Because wavelength (22 m) at 13.56 MHz is large, the phase of the magnetic field remains nearly constant within the operating range of the TX

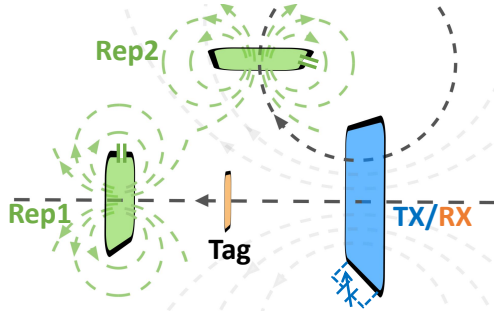

Figure 11: TX coil, mag-repeater placement and magnetic field line from TX coil and mag-repeater.

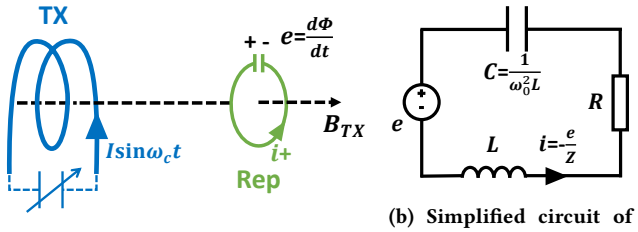

(a) Mag-repeater excited by a TX coil. **(b) Simplified circuit of mag-repeater.**

Figure 12: Simplified circuit model of mag-repeater.

coil. Therefore, as shown in Fig. 12b, the magnetic flux produced at the repeater by a current $I sin\omega_c t$ on the TX coil can be written as $\Phi sin\omega_c t$, where $\Phi = B_{TX}\pi R_{rep}^2$ and B_{TX} is the average magnetic field strength passing through the mag-repeater's coil. The time-varying magnetic flux induces an electromotive force in the repeater coil following Maxwell's equation [25]. Along the positive direction of the magnetic flux in Fig. 12, the electromotive force e is

$$e = \frac{d\Phi}{dt} = \omega_c \Phi cos\omega_c t, \tag{14}$$

which can be treated as an equivalent signal source. Therefore, we can model the passive mag-repeater as a serial RLC circuit driven by a voltage source as shown in Fig. 12b. Then the current through the inductor (the coil) becomes

$$i = -\frac{e}{Z} = -\frac{e}{j\omega_c L + R_s + \frac{\omega_0^2 L}{j\omega_c}} \tag{15}$$

where ω_0 is the resonant frequency of the mag-repeater, which will impact how the mag-repeater collaborates with the TX coil.

Let's take a look at the normalized amplitude and differential phase response of the current on the repeater with respect to a reader coil resonating at 13.56 MHz. Fig. 13a shows that the elicited current amplitude in a mag-repeater attains maximum when its resonant frequency is equal to that of a TX coil, and the amplitude response will quickly drop if the repeater's resonant frequency deviates from 13.56 MHz. Moreover, Fig. 13b shows that the phase of the signal elicited by the mag-repeater has a 90° phase difference compared to the 13.56 MHz signal from the TX coil when the repeater is resonating at 13.56 MHz. By taking $\theta_2(n) - \theta_1(n) = 90°$ in Eq. 10, the final power will be $\left(b_1(n,\mathcal{R},\beta)\right)^2 + \left(b_2(n,\mathcal{R},\beta)\right)^2$. This means the 90° phase difference does not introduce destructive combination although it deviates from the optimal phase combination discussed in Sec. 5.2. In fact, the gain on amplitude response when

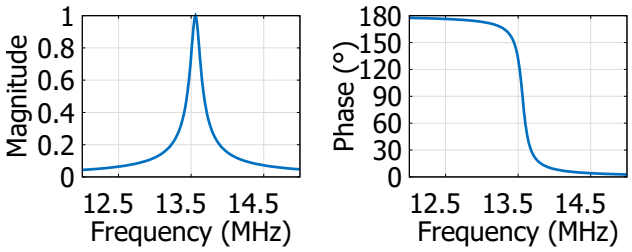

(a) Mag-repeater current magnitude response. **(b) Phase difference between TX coil and mag-repeater.**

Figure 13: Magnitude and differential phase response over frequency of a repeater with respect to a reader coil resonating at 13.56 MHz.

resonating at 13.56 MHz will be higher than the maximum constructive combination, because when the phase equals to 0 or π (repeater is resonating at higher or lower frequency) the amplitude response will drop a lot. So having the repeater resonating at the carrier frequency 13.56 MHz is a better choice when it is design for helping TX. Moreover, if the repeater is located in an appropriate region with a sufficient Q, its elicited currents can be as large as that in the original TX coil (several amps), which subsequently generate strong magnetic fields (can be even higher than that from the TX coils when the location is near to the repeater). With this modeling, *the passive mag-repeater acts equivalently as a TX coil*, introducing more diversity and helping eliminate "dead spots" undiscovered by the reader.

7 IMPLEMENTATION

In this section, we describe the implementation of NFC+, which consists of a multi-channel reader, high-Q resonant loop coils and passive mag-repeaters. The reader (shown in appendix.C) contains a TX module, an RX module and a central processing unit and runs the physical and MAC layer protocol.

TX module: The TX module supports 4 concurrent TX paths. It employs a phase controller that tune phase independently in each path to perform the magnetic beamforming (Sec. 5.2). The phase controller includes 4 flip-flop-based QPSK modulators that run on a 13.56 MHz × 4 = 54.24 MHz clock, which is generated from an ATF16V8A PLD to obtain different phase values. After the carrier with the desired phase value is generated, ASK modulation is applied to encode downlink data using RF switch. The output signal power delivered to TX coils is set at 5 W.

RX module: In the RX module, a 2-stage crystal notch filter with 13.56 MHz nulling-frequency is inserted before the amplification module to suppress the large self-jamming from TX. The notch filter uses air-core inductors to avoid saturation in order to achieve low insertion loss (measured 0.3 dB total). The signal output from the notch filter is amplified by a low noise amplifier (LNA) PHA-13HLN+ and then fed into an image-rejection LC bandstop filter. As discussed in Sec. 4.2, the standard NFC tag modulates on both sidebands at 13.11 MHz and 14.01 MHz. Therefore, we design NFC+'s RX module to be reconfigurable so that it can support two sets of configurations. These uplink sidebands are down-converted to an IF at 10.7 MHz for IF processing. We apply two 10.7±0.18 MHz

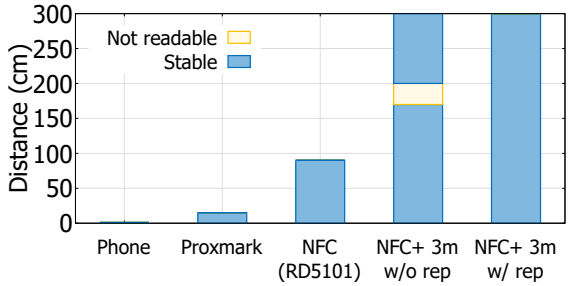

Figure 14: Maximum operational distance achieved by NFC on a smartphone, ProxMark, Andea Electronics RD5101 and NFC+.

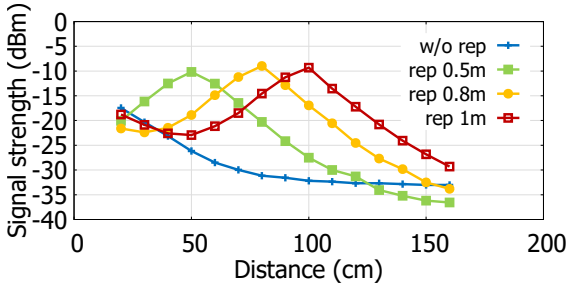

Figure 15: Mag-repeater helps improve the signal strength at long distances.

ceramic filters SFECF10M7GA00 to further attenuate the interference and reduce the noise bandwidth. We use a 16-bit ADC to sample the IF signals. The digital samples are processed by the controller which performs digital filtering, frame synchronization, and coherent demodulation.

Protocol & processing unit: The processing unit is an STM32 ARM Cortex-M7 MCU, in which we implement ISO 15693 [26] compatible physical-layer (de-)modulation and MAC-layer protocol in C++. The MAC protocol implements collision detection and can support >50 tag/s read-rate which is sufficient for logistic applications. All modules are clocked from single PLL-DLL clock generator Si5351A which provides multiple clock frequencies derived from one crystal reference. This reference clock sharing helps avoid the carrier frequency offset issue in the tag signal decoding.

High-Q coils: The resonant TX/RX coils use aluminum gamma-loop [27]. Each coil has a 0.9 m×1.1 m dimension, high power rating, and a tunable Q value up to 300 which perfectly satisfies our high Q and high power requirement.

Mag-repeater: The repeater loop is a customized one-turn loop using a copper tube with a diameter of 9.42 mm. It is connected to a PCB board with external (variable) shunt and series capacitors for tuning and impedance-matching.

Tags: NFC+ communicates with *standard low-cost battery-free NFC tags that support ISO 15693*, such as the NXP ICODE and the MIFARE family [28].

8 EVALUATION

In this section, we will show NFC+ can read commercial NFC tags at different distances and various orientations.

8.1 NFC+'s operational distance

We compare the reading range of NFC+ against 3 baseline NFC systems: a smartphone NFC reader [29], Proxmark [30] (an open-source NFC reader that has evolved over 10 years), and Andea Electronics RD5101 [15] (a commercial NFC reader that claims decimeter level reading range). Fig. 14 summarizes the results. Since the smartphone, Proxmark, and RD5101 use only one coil for both transmission and reception, we place a tag parallel to the coil (i.e., the most favorable orientation) and gradually move the tag away. Then, we measure whether the tag can be read across distances.

The smartphone can only read tags around 1 cm away because it is primarily used for secure payment which does not operate at a long distance. Proxmark can read tags at a distance of no more than 15 cm. As a result, it is mainly used as a tool for the sniffer and debugging. To our knowledge, RD5101 reaches the longest reading range of NFC reader. Using 8 W output power and an 80 cm×50 cm coil, RD5101 can read tags up to 90 cm away, which is still not sufficient for the 2.5 m range needed by many logistics network applications. Note that current RD5101 hardware only supports one coil. Therefore, it cannot leverage the high Q coils used in NFC+ since the communication symbols is distorted due to the narrow bandwidth. Moreover, even if RD5101's hardware is modified to support two coils, one for transmission and one for reception, its reception sensitivity is not sufficient due to lack of self-interference cancellation.

Since NFC+ support multiple coils, we place one RX coil 3 m away from the TX coil. Then, we place a tag between the TX and RX coils and move it away from the TX coil. When the repeater is not used, the tag can be read when it is 0~170 cm and 200~300 cm away from the TX coil. Tag inventory fails for distance 170~200 cm because the summation of the downlink and uplink budget is the smallest at these locations.

Then, we place a mag-repeater between TX and RX coils and keep the repeater to tag distance as 50 cm. With this setup, NFC+ can consistently read tags across the whole 3 m region between the TX and RX coils. This *reliable operational distance* is 3× longer than RD5101, 20× over Proxmark and 300× over the smartphone NFC reader. Therefore, NFC+ is the first system that can operate at a relatively long distance that enables the inventory of bulk commodities in retail/warehouse settings.

To understand how a mag-repeater helps improve the operational distance of NFC+, we place a mag-repeater 0.5 m, 0.8 m, and 1 m away and in parallel to the TX coil. Then, we increase the TX-tag distance and measure the power received by the tag using a pickup loop. As Fig. 15 shows, without the mag-repeater, the received power decreases monotonically over distance. However, with a mag-repeater, the received power is significantly improved by 16-23 dB, and maximized when the tag is close to the mag-repeater. Improvements occurs within ±50 cm range of the repeater.

8.2 Handling undesired orientation

We also benchmark NFC+'s performance when tags are placed with different orientations. As Fig. 9 shows, we place two TX coils (TX1 and TX2) perpendicular to each other and separated by 1.75 m from center to center. Then, we place two RX coils parallel to the TX coils with the same distances of 2.5 m. An NFC tag is further placed at the center (tag2 location in Fig. 9).

Table 1: Signal strength degradation when a NFC or UHF tag is attached to different products.

Products	Bottle water		Can coke		Bottle Coke		Boxed milk 1		Boxed milk 2		Bottle Beer	
Tag location	front	back	front	back	front	back	front	back	front	back	front	back
NFC+	0dB	0dB	6.6dB	8.6dB	0dB	0dB	5.6dB	7.6dB	2.5dB	4.3dB	0dB	0dB
UHF	9dB	24dB	13dB	24dB	14dB	21dB	16dB	26dB	4dB	16dB	6dB	14dB

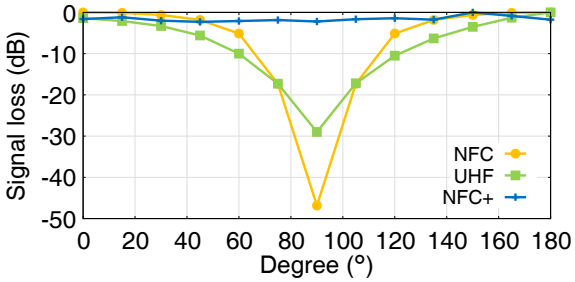

Figure 16: Performance of NFC+, state-of-the-art NFC, and UHF RFID with different tag orientations.

(a) Warehouse deployment **(b)** Supply chain deployment

Figure 17: Deploying NFC+ in practical logistic networks.

Fig. 16 shows the loss of signal experienced by a tag compared to its optimum orientation. Signal loss is chosen to compare the performance of heterogeneous NFC, UHF and NFC+ platforms. We can see that NFC+'s tag harvests a strong magnetic flux from TX coils and repeater. Even in the worst case, it only experiences around 3 dB signal strength degradation, i.e., *NFC+'s signal quality is almost invariant to the tag orientation*[6].

As a comparison, we evaluate the performance of RD5101 NFC and UHF RFID when the reader sits at TX1 in Fig. 9 and the tag sits at the same location as the NFC+ tag. We can see that both the UHF RFID tag and NFC tag experience more than 30 dB signal strength loss when its antenna is perpendicular (90°) to the reader antenna. As a result, it is very hard for the UHF RFID reader and RD5101 NFC reader to read tags that are misoriented at around 90°.

8.3 Comparing NFC+ and UHF RFID

We now compare the performance of NFC+ and UHF RFID when the tags are attached to the front and backside of various products, corresponding to LoS and NLoS between the reader and tag. Table 1[7] summarizes the signal strength difference when the tag is or is not attached to a product.

When the NFC tag is attached to liquid products, such as bottled water, coke, and beer, the received power does not degrade at all. In contrast, UHF suffers from 4-16 dB degradation even under LoS, and much larger (14-26 dB) when the tag is attached to the back of the product. Such a low signal quality makes the UHF tags unreadable even at a short range. The received power of NFC+ degrades when the tag is attached to metallic products, such as Can Coke (6.6-8.6 dB loss) and boxed milk whose packages contain metallic materials. Nonetheless, NFC+'s power degradation is much smaller compared to UHF tags. In addition, as in typical magnetic NFC systems, the problem can be alleviated by simply adding a thin substrate layer [31] between the NFC tag and the product. Such a substrate is well-known and we will not cover its design in paper.

[6]This result happens at a specific location where the strength from multiple coils are balanced. For other locations where the direction and amplitude of magnetic field are changed, the amplitude $b_i(n, \mathcal{R}, \beta)$ will not be the same. Then, the combined strength result will not be that flat. But it will still have a larger absolute strength comparing to the single coil setup because of the constructive combination.

[7]Boxed milk 1 and boxed milk 2 are both packaged in aluminum foil, but the package sizes are different.

9 LOGISTIC NETWORK EVALUATION

We evaluate NFC+ in a warehouse and a supply chain settings, as illustrated in Fig. 17, to understand its performance in practical logistics networks.

9.1 Warehouse deployment

In the warehouse setting, the NFC+ reader's coils are embedded on the left, right and top part of the scanning gate, while the mag-repeater is integrated into the blue moving cart shown in Fig. 17a. We used over 10,000 tags and attached them to various products that are stored and shipped in the warehouse, including water, milk, cans, beer, bread, oil, etc. Then, we place these products on a moving cart (Fig. 17a). The number of products per cart varies depending on the shipping volume, and their orientations are random. We do see some cases where a tag is closely packed between two products, e.g., boxed milk and a box of bottled water. We push the cart through the scanning gate and record the products read by NFC+.

Fig. 18 shows NFC+'s performance. We observe that NFC+ can read over 1-0.03%=99.97% of the tags passing through the gate. Much better than the commercial RD5101 NFC system which only reads 1-40%=60%. When UHF tags are placed on purpose, i.e., all tags have LoS with the reader, the UHF RFID system can read 1-1.54%=98.46% of the products. Even though the reading rate seems close to the 99.9% requirement of many logistic applications, such minor tailing error may translate into non-trivial revenue loss for the big warehouses. Moreover, ensuring LoS tag placement costs lots of labor and cannot be guaranteed in practical deployment due to labor shortage and unprofessional worker operation. When products are placed with random orientation, the miss-reading rate of UHF RFID jumps from 1.54% to 23% due to its low reliability under NLoS.

To evaluate the cross-reading rate, we define a 4 m×4 m ROI surrounding the TX and RX coil/antenna, and then place tags randomly around the border. From the result in Fig. 18b, we can see that neither NFC+ nor the commercial NFC read ANY tag that sits beyond the ROI. In contrast, the UHF RFID experiences a 42% cross-reading rate. The poor cross-reading performance is an inevitable sacrifice when the UHF RFID is tasked to achieve a high reading rate for tags in the ROI, especially those misoriented ones.

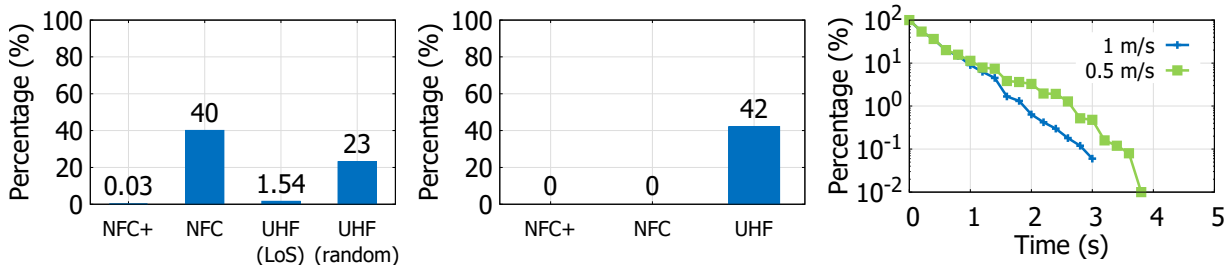

(a) Miss-reading rate. (b) Cross-reading rate. (c) Miss-reading rate over time.

Figure 18: NFC+'s performance in a warehouse. Over 10k tags are used. NFC+ can read over 1-0.03%=99.97% desired tags and does not any undesired tags. In comparison, commercial NFC systems and UHF RFID suffers from severe miss-reading or cross-reading.

In summary, NFC+ is the only system that can achieve over 99.9% accuracy when reading desired tags placed within the ROI while not reading ANY undesired tags outside the ROI. We are unaware of any RFID system that has proven to simultaneously achieve low miss-reading and cross-reading rate, with a large number and diverse type of products. Therefore, we believe that NFC+ is the correct approach for building the next generation of logistic networks.

An additional observation from our experiments is that the speed of a moving cart impacts NFC+'s performance. As summarized in Fig. 18c, when the cart passes through the gate at 1 m/s, NFC+ achieves less than 0.1% miss-reading rate (over 99.9% accuracy) within around 2.8 seconds. At a slower speed of 0.5 m/s, NFC+ can achieve less than 0.01% miss-reading rate (over 99.99% accuracy) within around 3.6 seconds. The results imply that slower moving speed does help reduce the miss-reading rate. Such a result is expected for the following two reasons: (1) The magnetic fields form closed loops so when an object traverses the fields, it "sees" more diversified angular coverage. (2) The reader samples tags at a rate of 50-tags/s. Therefore, for a specific tag, a slower motion means more opportunities to be sampled at different orientations which helps reduce miss-reading rate. It is worth noting that the time needed by the reader to sample a tag is on the order of milliseconds which translates to a spatial displacement of several millimeters when cart motion is involved. Therefore, regular motion will not interrupt NFC communication session because the magnetic strength is almost invariant during a specific sampling period. From the result, even with a faster speed of 1 m/s, NFC+'s miss-reading rate is still much lower than the NFC and UHF RFID systems.

9.2 Supply chain deployment

We also evaluate NFC+'s performance in a supply chain system where products in a water tank pass through a conveyor scanning gate, as illustrated in Fig. 17 (b). Fig. 19 shows the signal strength degradation when the tag is immersed at different levels of depth (in water), in comparison with an empty tank. We can see that NFC+'s magnetic signal does not degrade a lot as water depth increases. For example, when the tag is 15cm away from the edge of the water tank, the signal degradation is only 3dB, close to its airborne path loss. However, a UHF tag at the same location experiences more than 30dB signal degradation which fails the RFID operation. This experiment epitomizes NFC+'s capability to operate in a harsh environment where UHF RFID ceases to operate.

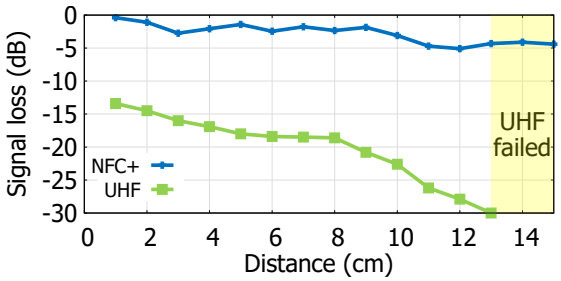

Figure 19: Signal degradation when tags are immersed in water. NFC+'s signal does not degrade a lot over distance while UHF RFID signal degrades significantly.

10 RELATED WORK

RFID communication: RFID has been considered as a key enabler for numerous IoT applications [32, 33]. However, through substantial efforts in realistic deployments over the past years, reliability issues of RFID have been discovered and widely reported by industry practitioners [34–37]. The read rate of RFID was found to be dramatically reduced by the contents of a package. For example, [35] reported that only 25% of tags on containers of water bottles could be read. The readability and range is also heavily impacted by tag orientation [38]. In addition to the miss-reading problem caused by unfriendly materials, another challenge was found to be the cross-reading error [39]. In fact, one major motivation of RFID localization was to address the cross-reading error [40–42] so that out-of-range tags could be excluded. Unfortunately, past localization works could not solve the problem. They not only required moving tags to combat multi-paths, but also could only localize tags in LoS conditions. So they were not applicable to complex industrial environments, especially for applications that require high reliability. Another line of research tried to improve the efficiency of RFID protocols [43] and extending the communication distance via beam-forming techniques [44]. However, these works were mainly based on algorithmic innovations and hence could not address the reliability issue that roots in the physical nature of the technology. In contrast, NFC+ takes a fresh look at this problem and addresses the above challenges with both physical and algorithmic innovations.

Backscatter networking: Both RFID and NFC rely on the physical principle of backscatter. Backscatter networking have also gained a lot of attention in recent years [45, 45–48]. The low power

nature [49] of backscatter made it unique to enable new applications ranging from machine-to-machine communications [46], low-power and low-cost WiFi connectivity [50] to in-body and on-body communications [47–49]. Unlike NFC+, past proposals extended backscatter principle to novel applications, so the reliability of RFID applications was not their focus. In addition, in order to optimize their specific usages, most of these proposals relied on customized circuit or antennas on the tag side. In contrast, NFC+ is fully compatible with ISO 15693 which is supported by most of today's commercial NFC chips, so it does not require changing NFC tags. Therefore, NFC+ is a ready-to-deploy solution which can be directly applied to many RFID applications.

Magnetic wireless power transfer: NFC+ is also closely related to magnetic wireless power transfer [51–53]. Magnetic wireless power transfer was initially discovered by Nikola Tesla in 1914 [51]. Tesla designed tesla-coils to show that energy could be moved efficiently between these coils when strong inductive coupling was present. It was later discovered that [52] via strong magnetic resonance, efficient energy transfer could also be obtained even under weak inductive coupling conditions. In addition to leveraging resonance, other researchers proposed to use multiple coils [54–56] to beam-form energy. For example, MagMIMO [54, 57] showed that one could use multiple coils to charge a cellphone more efficiently than a regular single-coil charging pad. NFC+ leverages the knowledge from these past works but differs in the following aspects. *First*, none of the past systems was designed to work with miniaturized passive devices like NFC tags. In NFC+, the resonance effect on the tag side is usually very limited so it cannot establish strong resonant coupling with the transmit coil like what was needed in [52]. *Second*, in NFC+, we must charge a large number of devices at the same time but unlike a cellphone, these devices are passive and therefore, it is not feasible to obtain the the feedback matrix from them and use iterative beam-forming algorithm as described in [57]. *Last*, the goal of these past proposals was purely wireless charging. They delt with only transmitting but not receiving, so they did not have to satisfy the constraints required by both power link and data link that NFC+ handles at the same time.

11 DISCUSSIONS

Tag Costs: Recent breakthroughs have brought the cost of an NFC tag down to $5 cents [7]. We expect the cost of an NFC tag to further shrink if it is applied to logistic networks for the following reasons: (1) The volume of tags needed by logistic networks is extremely large [1], which will drive down the cost [58]. (2) The minimum length of memory required by logistics (96-bit GID [59]) is much less than what is needed in contact-less payments, which means much smaller die size for an NFC chip and hence lower cost. Therefore, there is a strong economic incentive for logistics network to adopt NFC instead of UHF RFIDs.

Reader Costs: The amortized deployment cost of practical RFID readers is always much less than that of RFID tags, because one reader can be used to read millions of tags. Hence, for logistic network applications, the cost of readers is usually considered negligible. In our prototype, the customized manufacturing cost of NFC+ reader is about $1000. The additional cost compared to commercial NFC is due to the specialized multi-coil design and dedicated high sensitivity receiver design. However, we would like to point out that as the reader is built with off-the-shelf chips and components, we expect the cost to shrink drastically once NFC+ is moved into mass production.

Human Safety: The signal used by NFC+ is a non-radiating magnetic field and the strength required to activate a NFC tag is $0.15A/m$ or $0.19\mu T$ [26], much lower than the head and limb safety limits of $0.205mT$ specified by IEEE standard [60]. NFC+'s reader supports 4 TX channels with 5 W peak output power per channel, consuming a total power around 20 W, which is smaller than commercial wireless charging devices such as Witricity WiT-2000M and Energizer Qi [54].

Design trade-off: We choose to use high-Q coil to improve the range coverage. However, higher Q leads to narrower bandwidth, which means the coil will need more careful tuning and can be more sensitive to the environments (e.g., its resonating frequency may be affected by temperature). To address these issues, a typical solution in magnetic communication is to use a smart auto-tuner [18], i.e., a servomotor that rotates the shaft of the vacuum capacitor according to Standing Wave Ratio (SWR) sensor readout. We leave such enhancement for our future work.

Reading rate: We use unmodified standard ISO 15693 tags. This NFC standard mandates a binary-tree MAC protocol to resolve collision between tags. It allows a reading rate of up to 50 tags/s, which we found to be sufficient for typical logistic applications. Existing research has investigated techniques to improve the reading rate, but these are beyond the scope of our work.

New applications enabled by NFC+: We envision the techniques introduced by NFC+ to enable a variety of novel applications. First, NFC+ enables digital-IDs to be applied in not only the entire lifecycle of a supply chain, but also the interaction with end-consumers. Today's smart phones such as iPhones are already equipped with NFC capabilities, so customers are able to directly obtain logistic information once NFC is used to manage supply chain at large-scale. In addition, as magnetic signals can easily traverse human body, NFC+ opens new opportunities to achieve deep-tissue power delivery and communication with implantable devices for medical applications [47, 48].

12 CONCLUSION

In summary, we present the design and implementation of NFC+, the first system that can do RFID tag inventory with sufficient accuracy and high reliability. NFC+ leverages magnetic field to ensure that it can read 99.9% tags within ROI, even when these tags are attached to or blocked by RFID unfriendly objects, such as milk, cans, water, etc. In addition, NFC+ does not cross-read ANY tag that sits outside the ROI. Our large-scale evaluation in a warehouse shows that NFC+ not only enables using RFID in logistics networks but also paves the way for other other novel applications such as automated new retail and implantable medical devices. **Claim**: This work does not raise any ethical issues.

ACKNOWLEDGMENTS

We thank the anonymous reviewers and shepherd for their insightful comments and feedback.

REFERENCES

[1] Parcel Pending. Package Delivery Statistics: A Global Perspective. https://www.parcelpending.com/blog/package-delivery-statistics/, 2018.

[2] Impinj. Accurate Inventory Visibility with RAIN RFID. https://www.impinj.com/library/blog/2020-in-2020-accurate-inventory-visibility-with-rain-rfid, 2019.

[3] Carla R Medeiros, Jorge R Costa, and Carlos A Fernandes. Rfid reader antennas for tag detection in self-confined volumes at uhf. *IEEE Antennas and Propagation Magazine*, 53(2):39–50, 2011.

[4] Ju Wang, Liqiong Chang, Omid Abari, and Srinivasan Keshav. Are rfid sensing systems ready for the real world? In *Proceedings of the 17th Annual International Conference on Mobile Systems, Applications, and Services*, pages 366–377, 2019.

[5] Texas Instrument. Antenna design guide for the trf79xxa. http://www.ti.com/lit/an/sloa241b/sloa241b.pdf, February 2018.

[6] Melexis Inc. 13.56 mhz rfid systems and antennas design guide. https://www.limpkin.fr/public/NFC/RFID_antennas.pdf, 2004.

[7] NXP. Nxp and identiv announce breakthrough in nfc tag pricing. https://www.nfcw.com/2019/02/05/361215/nxp-and-identiv-announce-breakthrough-in-nfc-tag-pricing, 2019.

[8] Mohsen Shahmohammadi, Matt Chabalko, and Alanson P Sample. High-q, over-coupled tuning for near-field rfid systems. In *2016 IEEE International Conference on RFID (RFID)*, pages 1–8. IEEE, 2016.

[9] Sunil K Timalsina, Rabin Bhusal, and Sangman Moh. Nfc and its application to mobile payment: Overview and comparison. In *2012 8th International Conference on Information Science and Digital Content Technology (ICIDT2012)*, volume 1, pages 203–206. IEEE, 2012.

[10] Florian Pfeiffer, Klaus Finkenzeller, and Erwin Biebl. Theoretical limits of iso/iec 14443 type a rfid eavesdropping attacks. In *Smart SysTech 2012; European Conference on Smart Objects, Systems and Technologies*, pages 1–9. VDE, 2012.

[11] Thomas H Lee. *The design of CMOS radio-frequency integrated circuits*. Cambridge university press, 2003.

[12] Constantine Balanis. *Antenna Theory: Analysis and Design*, chapter 5, pages 235–284. John wiley & sons, 2016.

[13] Carl R. Nave. Magnetic field of current loop. http://hyperphysics.phy-astr.gsu.edu/hbase/magnetic/curloo.html#c4.

[14] The Clemson University Vehicular Electronics Laboratory. Inductance Calculator. https://cecas.clemson.edu/cvel/emc/calculators/Inductance_Calculator/circular.html, 2020.

[15] Ltd. Guangzhou Andea Electronics Technology Co. Cots long range nfc reader. http://en.gzandea.com/English/Products/126, 2015.

[16] Raymond M Fish and Leslie A Geddes. Conduction of electrical current to and through the human body: a review. *Eplasty*, 9, 2009.

[17] F.Dörenberg. Small magnetic transmitting loop. https://www.nonstopsystems.com/radio/frank_radio_antenna_magloop.htm, 2015.

[18] Frank Dörenberg. Small "magnetic" transmitting loop for 80-20 mtrs. https://www.apple.com/iphone-11/specs/.

[19] Voyantic. Tagformance pro. https://voyantic.com/products/tagformance-pro.

[20] Texas Instruments. Trf7970a multiprotocol fully integrated 13.56-mhz rfid and near field communication (nfc) transceiver ic. *Datasheet, SLOS743L–REVISED MARCH*, 2017.

[21] Melanie R Rieback, Georgi Gaydadjiev, Bruno Crispo, Rutger FH Hofman, and Andrew S Tanenbaum. A platform for rfid security and privacy administration. In *USENIX LISA*, pages 89–102, 2006.

[22] Dinesh Bharadia, Emily McMilin, and Sachin Katti. Full duplex radios. In *Proceedings of the ACM SIGCOMM 2013 conference on SIGCOMM*, pages 375–386, 2013.

[23] Renjie Zhao, Timothy Woodford, Teng Wei, Kun Qian, and Xinyu Zhang. M-Cube: A Millimeter-Wave Massive MIMO Software Radio. In *Proceedings of the 26th Annual International Conference on Mobile Computing and Networking (MobiCom)*, New York, NY, USA, 2020.

[24] Yunfei Ma, Nicholas Selby, and Fadel Adib. Drone relays for battery-free networks. In *Proceedings of the Conference of the ACM Special Interest Group on Data Communication*, pages 335–347, 2017.

[25] MIT open courseware. Maxwell's equation, electromagnetic waves. https://ocw.mit.edu/courses/physics/8-03sc-physics-iii-vibrations-and-waves-fall-2016/part-ii-electromagnetic-waves/lecture-12/, 2015.

[26] ISO. Iso/iec 15693-2:2006 [iso/iec 15693-2:2006]. https://www.iso.org/standard/39695.html, 2006.

[27] Gary R Zanzig. Loop antenna with integral tuning capacitor, 1991. US Patent 5,072,233.

[28] NXP. Icode. https://www.nxp.com/products/rfid-nfc/nfc-hf/, 2019.

[29] Google. Pixel 4. https://store.google.com/product/pixel_4_specs.

[30] Proxmark. Open-Source NFC. https://proxmark.com, 2020.

[31] Byungje Lee, Byeongkwan Kim, Frances J Harackiewicz, Byeonggwi Mun, and Hyunwoo Lee. Nfc antenna design for low-permeability ferromagnetic material. *IEEE Antennas and wireless propagation letters*, 13:59–62, 2014.

[32] Konstantinos Domdouzis, Bimal Kumar, and Chimay Anumba. Radio-frequency identification (rfid) applications: A brief introduction. *Advanced Engineering Informatics*, 21(4):350–355, 2007.

[33] Yunfei Ma, Nicholas Selby, and Fadel Adib. Minding the billions: Ultra-wideband localization for deployed rfid tags. In *Proceedings of the 23rd Annual International Conference on Mobile Computing and Networking*, pages 248–260, 2017.

[34] Dan Gilmore. Did walmart's failed case tagging program set rfid back or move it forward? Supply Chain Digest, 2017.

[35] Robert H Clarke, Diana Twede, Jeffrey R Tazelaar, and Kenneth K Boyer. Radio frequency identification (rfid) performance: the effect of tag orientation and package contents. *Packaging Technology and Science: An International Journal*, 19(1):45–54, 2006.

[36] Sozo Inoue, Daisuke Hagiwara, and Hiroto Yasuura. Systematic error detection for rfid reliability. In *First International Conference on Availability, Reliability and Security (ARES'06)*, pages 7–pp. IEEE, 2006.

[37] Vidyasagar Potdar, Pedram Hayati, and Elizabeth Chang. Improving rfid read rate reliability by a systematic error detection approach. In *2007 1st Annual RFID Eurasia*, pages 1–5. IEEE, 2007.

[38] Teng Wei and Xinyu Zhang. Gyro in the air: tracking 3d orientation of batteryless internet-of-things. In *Proceedings of the 22nd Annual International Conference on Mobile Computing and Networking (MobiCom)*, pages 55–68, 2016.

[39] Miodrag Bolic, Majed Rostamian, and Petar M Djuric. Proximity detection with rfid: A step toward the internet of things. *IEEE Pervasive Computing*, 14(2):70–76, 2015.

[40] Lei Yang, Yekui Chen, Xiang-Yang Li, Chaowei Xiao, Mo Li, and Yunhao Liu. Tagoram: Real-time tracking of mobile rfid tags to high precision using cots devices. In *Proceedings of the 20th annual international conference on Mobile computing and networking*, pages 237–248, 2014.

[41] Longfei Shangguan and Kyle Jamieson. The design and implementation of a mobile rfid tag sorting robot. In *Proceedings of the 14th Annual International Conference on Mobile Systems, Applications, and Services*, pages 31–42, 2016.

[42] Jue Wang, Deepak Vasisht, and Dina Katabi. Rf-idraw: virtual touch screen in the air using rf signals. *ACM SIGCOMM Computer Communication Review*, 44(4):235–246, 2014.

[43] Jue Wang, Haitham Hassanieh, Dina Katabi, and Piotr Indyk. Efficient and reliable low-power backscatter networks. *ACM SIGCOMM Computer Communication Review*, 42(4):61–72, 2012.

[44] Jingxian Wang, Junbo Zhang, Rajarshi Saha, Haojian Jin, and Swarun Kumar. Pushing the range limits of commercial passive rfids. In *USENIX Symposium on Networked Systems Design and Implementation (NSDI)*, pages 301–316, 2019.

[45] Pengyu Zhang, Jeremy Gummeson, and Deepak Ganesan. Blink: A high throughput link layer for backscatter communication. In *Proceedings of the 10th international conference on Mobile systems, applications, and services*, pages 99–112, 2012.

[46] Vincent Liu, Aaron Parks, Vamsi Talla, Shyamnath Gollakota, David Wetherall, and Joshua R Smith. Ambient backscatter: Wireless communication out of thin air. *ACM SIGCOMM Computer Communication Review*, 43(4):39–50, 2013.

[47] Deepak Vasisht, Guo Zhang, Omid Abari, Hsiao-Ming Lu, Jacob Flanz, and Dina Katabi. In-body backscatter communication and localization. In *Proceedings of the 2018 Conference of the ACM Special Interest Group on Data Communication*, pages 132–146, 2018.

[48] Yunfei Ma, Zhihong Luo, Christoph Steiger, Giovanni Traverso, and Fadel Adib. Enabling deep-tissue networking for miniature medical devices. In *Proceedings of the 2018 Conference of the ACM Special Interest Group on Data Communication*, pages 417–431, 2018.

[49] Pengyu Zhang, Mohammad Rostami, Pan Hu, and Deepak Ganesan. Enabling practical backscatter communication for on-body sensors. In *Proceedings of the 2016 ACM SIGCOMM Conference*, pages 370–383, 2016.

[50] Bryce Kellogg, Aaron Parks, Shyamnath Gollakota, Joshua R Smith, and David Wetherall. Wi-fi backscatter: Internet connectivity for rf-powered devices. In *Proceedings of the 2014 ACM conference on SIGCOMM*, pages 607–618, 2014.

[51] Nikola Tesla. Apparatus for transmitting electrical energy., December 1 1914. US Patent 1,119,732.

[52] Andre Kurs, Aristeidis Karalis, Robert Moffatt, John D Joannopoulos, Peter Fisher, and Marin Soljačić. Wireless power transfer via strongly coupled magnetic resonances. *science*, 317(5834):83–86, 2007.

[53] Joaquin J Casanova, Zhen Ning Low, and Jenshan Lin. A loosely coupled planar wireless power system for multiple receivers. *IEEE Transactions on Industrial Electronics*, 56(8):3060–3068, 2009.

[54] Jouya Jadidian and Dina Katabi. Magnetic mimo: How to charge your phone in your pocket. In *Proceedings of the 20th annual international conference on Mobile computing and networking*, pages 495–506, 2014.

[55] Steven Kisseleff, Ian F Akyildiz, and W Gerstacker. Beamforming for magnetic induction based wireless power transfer systems with multiple receivers. In *2015 IEEE Global Communications Conference (GLOBECOM)*, pages 1–7. IEEE, 2015.

[56] Nikolay Tal, Yahav Morag, and Yoash Levron. Magnetic induction antenna arrays for mimo and multiple-frequency communication systems. *Progress In Electromagnetics Research*, 75:155–167, 2017.

[57] Lixin Shi, Zachary Kabelac, Dina Katabi, and David Perreault. Wireless power hotspot that charges all of your devices. In *Proceedings of the 21st Annual International Conference on Mobile Computing and Networking*, pages 2–13, 2015.
[58] Randy H. Katz. Cost, price, and price for performance. http://bnrg.eecs.berkeley.edu/~randy/Courses/CS252.S96/Lecture05.pdf, 1996.
[59] Daniel D Deavours. Uhf epc tag performance evaluation. *RFID Journal [Online], May*, 2005.
[60] IEEE Standards Coordinating Committee. Ieee standard for safety levels with respect to human exposure to radio frequency electromagnetic fields, 3khz to 300ghz. *IEEE C95. 1-1991*, 1992.

APPENDIX

Appendices are supporting material that has not been peer reviewed.

A COUPLING BETWEEN MULTIPLE TX COILS

In this section, we discuss the influence of TX coils mutual coupling and how to deal with it.

In the long range NFC communication scenario, the value of TX to tag coupling is pretty small compared to the inter-TX magnetic couplings. Therefore, the influence of the tags to a reader coil's impedance is negligible and the behaviour of TX coils can be simply modeled as:

$$\text{TX Equation:} \quad \vec{v}_T = Z_T \vec{i}_T \tag{16}$$

where $\vec{v}_T$ and $\vec{i}_T$ are the TX voltages and currents, Z_T is the TX impedance and inter-TX magnetic couplings.

In the near field, the amplitude and phase of magnetic field is determined by the TX currents $\vec{i}_T$. Therefore, we need to control the amplitude and phase of $\vec{i}_T$ to achieve the magnetic field control as discussed in Sec. 5.2. However, in the practical hardware implementation of reader, the supply which we can directly control is $\vec{v}_T$. Since the complex matrix Z_T will introduce phase and amplitude distortion from $\vec{v}_T$ to $\vec{i}_T$, the phase and amplitude in $\vec{v}_T$ will not result in the same phase and amplitude in $\vec{i}_T$.

Theoretically, when we know the value of Z_T, the influence of TX coupling can be compensated by having flexible control on the TX coils input like in [57].

B MAGNETIC BEAMFORMING

In this section, we describe the details on how to get Eq. 10 from Eq. 9. We drop n, $\mathcal{R}$ and β for simplicity. Since the signal we look at is the magnetic signal, it generates an electromotive force on the tag. Following the Faraday's law of induction, the tag's received signal is proportional to the dot product of combined vector $\vec{H}_s$ in Eq. 10 and the unit normal vector of tag plane $\vec{e}_\beta$, i.e.:

$$\begin{aligned} R_{tag} =& S_1 a_1 sin(\omega t + \phi_1)(cos\alpha_1 cos\beta + sin\alpha_1 sin\beta) + \\ & S_2 a_2 sin(\omega t + \phi_2)(cos\alpha_2 cos\beta + sin\alpha_2 sin\beta) \\ =& S_1 a_1 cos(\alpha_1 - \beta) sin(\omega t + \phi_1) + \\ & S_2 a_2 cos(\alpha_2 - \beta) sin(\omega t + \phi_2) \end{aligned} \tag{17}$$

where S_i is the factor in Faraday's law of induction which is corresponding to the properties of the tag, such as coil size, number of turns etc. Take ϕ_1 as reference and $b_i(n, \mathcal{R}, \beta) = S_i k_i A_i cos(\alpha_i - \beta)$, we can get

$$\begin{aligned} R_{tag} =& b_1 sin(\omega t) + b_2 sin(\omega t + \phi_2 - \phi_1) \\ =& \big(b_1 + b_2 cos(\phi_2 - \phi_1)\big) sin\omega t + \big(b_2 sin(\phi_2 - \phi_1)\big) cos\omega t \end{aligned} \tag{18}$$

Figure 20: Photo of the NFC+'s reader PCB

For a signal $xsin\omega t + ycos\omega t$, the power is equal to $x^2 + y^2$. Therefore, we obtain Eq. 10 from Eq. 18.

C READER PCB

Fig. 20 gives the photo of the reader PCB. It contains the TX module, RX module, Crystal self-jamming cancellation and the ARM processor which runs NFC protocol as discussed in Sec. 7.